86-10783). We are grateful for advice from Drs J. C. Wittmann and B. Lotz concerning specimen preparation.

References

BASSETT, D. C. & HODGE, A. M. (1978). *Proc. R. Soc. London Ser. A*, **359**, 121–132.

BUNN, C. W. (1939). *Trans. Faraday Soc.* **35**, 482–491.

COWLEY, J. M. (1961). *Acta Cryst.* **14**, 920–927.

COWLEY, J. M. & MOODIE, A. F. (1957). *Acta Cryst.* **10**, 609–619.

COWLEY, J. M. & MOODIE, A. F. (1959*a*). *Acta Cryst.* **12**, 353–359.

COWLEY, J. M. & MOODIE, A. F. (1959*b*). *Acta Cryst.* **12**, 360–367.

COWLEY, J. M., REES, A. L. G. & SPINK, J. A. (1951). *Proc. Phys. Soc. London Sect. A*, **64**, 609–619.

DORSET, D. L. (1980). *Acta Cryst.* A**36**, 592–600.

DORSET, D. L. (1985). *J. Electron Microsc. Tech.* **2**, 89–128.

DORSET, D. L. (1986*a*). *J. Polym. Sci. Polym. Phys. Ed.* **24**, 79–87.

DORSET, D. L. (1986*b*). *Polymer*, **27**, 1349–1352.

DORSET, D. L. & MOSS, B. (1983). *Polymer*, **24**, 291–294.

DOYLE, P. A. & TURNER, P. S. (1968). *Acta Cryst.* A**24**, 390–397.

GOODMAN, P. & MOODIE, A. F. (1974). *Acta Cryst.* A**30**, 280–290.

HAMILTON, W. C. (1964). *Statistics in Physical Science*, p. 157. New York: Ronald Press.

HU, H., DORSET, D. L. & MOSS, B. (1988). *Ultramicroscopy*. In the press.

KAWAGUCHI, A., OHARA, M. & KOBAYASHI, K. (1979). *J. Macromol. Sci. Phys.* **16**, 193–212.

KEITH, H. D. & PADDEN, F. J. (1959). *J. Polym. Sci.* **39**, 101–123.

KERR, H. W. & LEWIS, M. H. (1971). *Advances in Epitaxy and Endotaxy*, edited by H. G. SCHNEIDER & V. RUTH, pp. 147–164. Leipzig: VEB Deutscher Verlag für Grundstoffindustrie.

MOSS, B., DORSET, D. L., WITTMANN, J. C. & LOTZ, B. (1985–1986). *J. Macromol. Sci. Phys.* **24**, 99–118.

O'KEEFE, M. A. & BUSECK, P. R. (1979). *Trans. Am. Crystallogr. Assoc.* **15**, 27–46.

PIESCZEK, W., STROBL, G. R. & MALZAHN, K. (1974). *Acta Cryst.* B**30**, 1278–1288.

WITTMANN, J. C., HODGE, A. M. & LOTZ, B. (1983). *J. Polym. Sci. Polym. Phys. Ed.* **21**, 2495–2509.

Acta Cryst. (1989). B**45**, 290–297

Charge Transfer and Three-Centre Bonding in Monoprotonated and Diprotonated 2,2′-Bipyridylium Decahydro-*closo*-decaborate(2−)

BY C. T. CHANTLER AND E. N. MASLEN

Crystallography Centre, University of Western Australia, Nedlands, Western Australia 6009, *Australia*

(*Received* 29 *September* 1987; *accepted* 16 *January* 1989)

Abstract

X-ray difference densities have been measured for the diprotonated form of the title compound at room temperature and for its monoprotonated analogue at 100 K. Atomic charges were determined by Hirshfeld's method of partitioning the difference density in proportion to atomic densities. Roughly 1·6 electrons are transferred to the $B_{10}H_{10}$ unit, and distributed widely over the cluster as a whole. That charge is less than the formal value of 2·0 electrons by an amount which correlates inversely with the strength of the interaction between the groups. The difference is not large, indicating that the cluster forms a robust, stable ionic species. Averaged difference densities in the B_3 rings resemble those reported by other workers. There is no evidence for open three-centre bonding. Closed three-centre bonds play a minor role in the redistribution of electron density. Asymmetric features in the difference maps are consistent with charge transfer resulting from close contact between B and N atoms. $C_{10}N_2H_{10}^{2+}.B_{10}H_{10}^{2-}$, $M_r = 276{\cdot}4$, monoclinic, $P2_1/c$, $a = 9{\cdot}937$ (4), $b = 10{\cdot}837$ (3), $c = 14{\cdot}856$ (5) Å, $\beta = 109{\cdot}21$ (3)°, $V = 1510{\cdot}6$ (9) Å^3, $Z = 4$, $D_x = 1{\cdot}22$ Mg m^{-3}, λ(Mo $K\alpha$) = 0·71069 Å, $\mu = 0{\cdot}0577$ mm^{-1}, $F(000) = 456$, $R = 0{\cdot}062$, $wR = 0{\cdot}047$ for 1771 observed reflections. $2C_{10}N_2H_9^+.B_{10}H_{10}^{2-}$, monoclinic, $P2_1/c$, $a = 11{\cdot}913$ (4), $b = 17{\cdot}656$ (5), $c = 11{\cdot}054$ (2) Å, $\beta = 101{\cdot}58$ (2)°, $V = 2278$ (2) Å^3, $Z = 4$, D_x 1·266 Mg m^{-3}, λ(Mo $K\alpha$) = 0·71069 Å, $\mu = 0{\cdot}0632$ mm^{-1}, $F(000) = 576$, $R = 0{\cdot}066$, $wR = 0{\cdot}045$ for 4524 observed reflections.

Introduction

Atomic charges can be determined from X-ray diffraction difference densities by the method of Hirshfeld (1977*a*,*b*). When applied to transition-metal complexes by Spadaccini (1988) and by Maslen, Ridout & Watson (1988), the results are remarkably consistent. The charges on individual atoms are smaller than the formal values, with magnitudes less than half an electron in most cases. On the other hand for polyatomic species such as hydrated metal ions the integrated charges are closer to the formal values. Consistent results were obtained even from diffraction experiments of structure determination quality, provided the data were not affected strongly by extinction (Maslen & Ridout, 1987).

If the error in the charge for a large molecular unit reflects the accumulation of uncorrelated uncertainties

0108-7681/89/030290-08$03.00

on the atomic charges, the total error would be large. Charges for chemically related moieties would be similar only by chance. The consistency of the charges determined for groups indicates partial cancellation of errors when summing the values for constituent atoms. These methods may be applicable to studies of charge transfer in crystalline solids generally. This can be tested by applying them to chemically related charge-transfer systems comprised of large units containing first-row atoms.

The diprotonated and monoprotonated bipyridylium salts of the $B_{10}H_{10}$ anion, which exhibit strong optical activity, were chosen to investigate charge transfer involving the boron clusters. Dipyridylium salts of the *closo*-decaborane anion show anomalous colour, attributed to a dynamic charge-transfer band by Muetterties, Balthis, Chia, Knoth & Miller (1964). The spectral properties indicate the nature and extent of the charge transfer. Before dynamic transfer can be fully described it is necessary to understand the static charge distribution. The $B_{10}H_{10}$ anion has a formal charge of -2 electrons, representing a transfer of negative charge to the cluster as a whole.

Clusters such as $B_{10}H_{10}^{2-}$, being electron deficient, are unable to provide a pair of valence electrons for each adjacent pair of atoms (Longuet-Higgins, 1949; Dixon, Klier, Halgren, Hall & Lipscomb, 1977). Thus electron pairs may be delocalized over several atomic centres. The concept of three-centre bonding attempts to overcome difficulties with earlier theories. Resonance hybridization of three-centre, two-electron bonds was the first and simplest extension of the normal two-centre bond to account for these clusters. A closed bond was defined to contain the bonding orbital within a roughly equilateral triangle formed by the three B atoms; an open three-centre bond based on an obtuse triangle was thought to have maximum density inside the obtuse angle. Other semi-empirical models of boron-cluster bonding have been developed to overcome deficiences in this model (Stone, 1981; Fuller & Kepert, 1983).

The degree of strain in the angles of closed ring systems is assessed by relating their instability and reactivity to the deviation from an ideal geometry. For the central atoms of the boron cluster there are six neighbours, so the ideal geometry is octahedral, but the bond angles are distorted, from 90° to roughly 60°, in the triangular faces due to cluster formation. The presence of strain should be indicated by distortion of the electron density distribution associated with bonding. A study of that distribution thus provides information on the nature of that bonding.

Experimental

The diprotonated 2,2′-bipyridylium salt of the *closo*-decaboron hydride anion $(LH_2)B_{10}H_{10}$, where L = 2,2′-bipyridyl = $C_{10}H_8N_2$, denoted REDCOP because of its intense red colour, and the corresponding monoprotonated salt $(LH)_2B_{10}H_{10}$, designated YELLOW, were synthesized from commercial-grade decaborane, $B_{10}H_{14}$, using triethylamine *via* the reaction $B_{10}H_{10} + Et_3N \rightarrow (Et_3NH)_2(B_{10}H_{10}) + H_2$, followed by addition of bipyridine in concentrated HCl.

Table 1. *Refinement details*

	REDCOP 295 K		YELLOW 100 K	
Crystal	Cuboid, 6 faces, 0·45 mm		Cuboid, 8 faces, 0·45 mm	
$2\theta_{max}$ (°)	50		60	
hkl range	$0 \le h \le 11, 0 \le k \le 12, -17 < l \le 16$		$0 \le h < 16, 0 \le k \le 24, -15 \le l \le 15$	
μ(Mo $K\alpha$) (mm^{-1})	0·0577		0·0632	
Intensity limit	$> 3\sigma$	All	$> 2\sigma$	All
N_{meas}	2559	2559	6637	6637
N_{ref}	1771	2559	4524	6637
R	0·062	0·074	0·066	0·099
wR	0·047	0·049	0·045	0·052
S	2·322		1·294	
$\Delta\rho_{max}$ (e Å^{-3})	0·25		0·44	
$\Delta\rho_{min}$ (e Å^{-3})	−0·27		−0·34	

Single-crystal X-ray diffraction data for REDCOP were measured at 295 K, using a Syntex $P\bar{1}$ four-circle diffractometer in ω–2θ scan mode with Mo $K\alpha$ radiation, $\lambda = 0{\cdot}71069$ Å. Details of the data collection and an initial refinement are given by Fuller, Kepert, Skelton & White (1987).

Because the absorption factor varies by only 2%, the corrections were not significant. The intensity of the low-angle 021 reflection, which had a count rate too great for the detector, was adjusted to that from refinement of the other reflections – a procedure equivalent to assigning zero weight to that reflection in the least-squares refinement. The two next most intense reflections (200 and $20\bar{2}$) showed a small amount of extinction (6%), but no others were affected significantly. This was corrected using default path lengths by the method of Zachariasen (1967). The extinction parameter r^* was 0·15 (2) (Larson, 1970), and the corrections were minor for all reflections other than 021, 200 and $20\bar{2}$.

The structure was refined using all reflections, with isotropic temperature factors for the H atoms and anisotropic temperature factors for all other atoms, by full-matrix least-squares methods using the *XTAL* system (Stewart & Hall, 1986) on a Perkin–Elmer 3240 computer, $w = \sigma^{-2}(|F|)$, until $\Delta/\sigma < 0{\cdot}01$.

For YELLOW (Fig. 1*b*), which was previously analysed using a limited set of room-temperature data by Fuller, Kepert, Skelton & White (1987), an extensive data set was measured at 100 K. The crystal had a small satellite crystal of the diprotonated species extending from the side of the main crystal. Its effect was significant for less than 0·01% of the reflections.

Absorption corrections were again insignificant, and no extinction was observed. Anisotropic thermal parameters were used for all atoms, including hydrogen, and refined by least-squares methods, $w = \sigma^{-2}(|F|)$, until $\Delta/\sigma < 0{\cdot}01$. The final refinement was

Table 2. *Fractional atomic coordinates and equivalent isotropic thermal parameters*

$$B_{eq} = (8\pi^2/3)\sum_i\sum_j U_{ij} a_i^* a_j^* \mathbf{a}_i.\mathbf{a}_j$$

	x	y	z	B_{eq}(Å²)
REDCOP				
B(1)	0·2668 (3)	0·2147 (3)	0·3577 (2)	2·77
H(1)	0·293 (2)	0·263 (2)	0·427 (1)	3·60
B(2)	0·3124 (3)	0·0712 (2)	0·3357 (2)	2·51
H(2)	0·381 (2)	0·014 (2)	0·394 (1)	2·63
B(3)	0·1266 (3)	0·1208 (2)	0·3062 (2)	2·56
H(3)	0·045 (2)	0·103 (2)	0·342 (1)	2·08
B(4)	0·1665 (3)	0·2570 (2)	0·2472 (2)	2·54
H(4)	0·113 (2)	0·351 (2)	0·232 (1)	2·44
B(5)	0·3518 (3)	0·2067 (3)	0·2763 (2)	2·60
H(5)	0·448 (2)	0·262 (2)	0·284 (1)	3·47
B(6)	0·3308 (3)	0·0549 (3)	0·2192 (2)	2·89
H(6)	0·426 (2)	0·008 (2)	0·213 (1)	2·97
B(7)	0·2290 (3)	0·1878 (3)	0·1562 (2)	2·85
H(7)	0·242 (2)	0·244 (2)	0·101 (1)	3·46
B(8)	0·0693 (3)	0·1290 (2)	0·1776 (2)	2·46
H(8)	−0·042 (2)	0·142 (2)	0·141 (2)	4·09
B(9)	0·1708 (3)	−0·0032 (2)	0·2405 (2)	2·55
H(9)	0·137 (2)	−0·093 (2)	0·256 (1)	2·30
B(10)	0·1717 (3)	0·0413 (3)	0·1319 (2)	2·91
H(10)	0·142 (2)	−0·007 (2)	0·062 (2)	4·00
N(1)*A*	0·7136 (2)	0·0337 (2)	0·1565 (1)	2·62
H(1)*A*	0·759 (2)	−0·031 (2)	0·187 (2)	3·25
C(2)*A*	0·6931 (2)	0·1333 (2)	0·2054 (2)	2·38
C(3)*A*	0·6285 (2)	0·2362 (2)	0·1558 (2)	2·66
H(3)*A*	0·610 (2)	0·303 (2)	0·187 (1)	2·51
C(4)*A*	0·5869 (2)	0·2357 (2)	0·0565 (2)	2·89
H(4)*A*	0·538 (2)	0·308 (2)	0·020 (1)	2·77
C(5)*A*	0·6135 (3)	0·1346 (2)	0·0100 (2)	3·13
H(5)*A*	0·587 (2)	0·131 (2)	−0·060 (2)	3·45
C(6)*A*	0·6780 (3)	0·0329 (2)	0·0611 (2)	3·05
H(6)*A*	0·708 (2)	−0·045 (2)	0·035 (2)	3·60
N(1)*B*	0·8168 (2)	0·2228 (2)	0·3590 (1)	2·73
H(1)*B*	0·832 (3)	0·292 (2)	0·328 (2)	5·01
C(2)*B*	0·7452 (2)	0·1239 (2)	0·3106 (2)	2·32
C(3)*B*	0·7301 (3)	0·0208 (2)	0·3598 (2)	2·93
H(3)*B*	0·677 (2)	−0·049 (2)	0·326 (2)	3·38
C(4)*B*	0·7908 (3)	0·0200 (2)	0·4586 (2)	3·52
H(4)*B*	0·778 (2)	−0·052 (2)	0·490 (2)	3·86
C(5)*B*	0·8672 (3)	0·1197 (2)	0·5057 (2)	3·66
H(5)*B*	0·912 (2)	0·123 (2)	0·577 (2)	5·06
C(6)*B*	0·8788 (3)	0·2219 (2)	0·4541 (2)	3·21
H(6)*B*	0·934 (2)	0·297 (2)	0·483 (2)	4·85
YELLOW				
B(1)	0·2680 (2)	0·2196 (1)	0·2662 (2)	1·37
H(1)	0·240 (2)	0·252 (2)	0·328 (2)	3·67
B(2)	0·2898 (2)	0·2390 (1)	0·1218 (2)	1·29
H(2)	0·274 (2)	0·296 (1)	0·086 (2)	2·14
B(3)	0·4034 (2)	0·2026 (1)	0·2451 (2)	1·23
H(3)	0·479 (2)	0·228 (1)	0·305 (2)	2·38
B(4)	0·3079 (2)	0·1264 (1)	0·2752 (2)	1·27
H(4)	0·307 (2)	0·095 (1)	0·358 (2)	1·70
B(5)	0·1942 (2)	0·1631 (1)	0·1537 (2)	1·36
H(5)	0·108 (2)	0·161 (1)	0·139 (2)	4·14
B(6)	0·2597 (2)	0·1586 (1)	0·0191 (2)	1·27
H(6)	0·203 (1)	0·168 (1)	−0·072 (2)	1·14
B(7)	0·2728 (2)	0·0789 (1)	0·1273 (2)	1·19
H(7)	0·229 (2)	0·022 (1)	0·123 (2)	2·37
B(8)	0·4205 (2)	0·1068 (1)	0·1919 (2)	1·24
H(8)	0·495 (2)	0·073 (1)	0·237 (2)	1·49
B(9)	0·4082 (2)	0·1860 (1)	0·0841 (2)	1·25
H(9)	0·469 (2)	0·217 (1)	0·044 (2)	1·99
B(10)	0·3704 (2)	0·0956 (1)	0·0374 (2)	1·40
H(10)	0·399 (1)	0·060 (1)	−0·027 (2)	1·55
N(1)1/*A*	0·3771 (1)	0·4356 (1)	0·1857 (1)	1·28
H(1)1/*A*	0·322 (2)	0·421 (1)	0·126 (2)	3·47
C(2)1/*A*	0·4252 (1)	0·5020 (1)	0·1638 (2)	1·25
C(3)1/*A*	0·5141 (2)	0·5293 (1)	0·2538 (2)	1·47
H(3)1/*A*	0·548 (2)	0·573 (1)	0·239 (2)	1·84
C(4)1/*A*	0·5504 (2)	0·4878 (1)	0·3607 (2)	1·65
H(4)1/*A*	0·617 (2)	0·504 (1)	0·425 (2)	2·48
C(5)1/*A*	0·4965 (2)	0·4203 (1)	0·3805 (2)	1·63
H(5)1/*A*	0·521 (2)	0·390 (1)	0·451 (2)	3·31
C(6)1/*A*	0·4075 (2)	0·3951 (1)	0·2893 (2)	1·56
H(6)1/*A*	0·365 (2)	0·350 (1)	0·292 (2)	1·97
N(1)1/*B*	0·2918 (1)	0·4982 (1)	−0·0268 (1)	1·41
C(2)1/*B*	0·3775 (1)	0·5380 (1)	0·0434 (2)	1·28
C(3)1/*B*	0·4175 (2)	0·6065 (1)	0·0075 (2)	1·64
H(3)1/*B*	0·475 (2)	0·636 (1)	0·058 (2)	2·30
C(4)1/*B*	0·3672 (2)	0·6357 (1)	−0·1079 (2)	1·85
H(4)1/*B*	0·392 (2)	0·682 (1)	−0·137 (2)	1·68
C(5)1/*B*	0·2795 (2)	0·5953 (1)	−0·1815 (2)	1·85
H(5)1/*B*	0·242 (2)	0·611 (1)	−0·267 (2)	2·33
C(6)1/*B*	0·2444 (2)	0·5276 (1)	−0·1364 (2)	1·64
H(6)1/*B*	0·185 (2)	0·501 (1)	−0·183 (2)	2·14
N(1)2/*A*	0·9724 (1)	0·3170 (1)	0·0573 (1)	1·48
H(1)2/*A*	0·941 (2)	0·286 (1)	−0·015 (2)	3·70
C(2)2/*A*	0·9520 (1)	0·2983 (1)	0·1686 (2)	1·25
C(3)2/*A*	0·9973 (2)	0·3430 (1)	0·2693 (2)	1·49
H(3)2/*A*	0·983 (2)	0·328 (1)	0·346 (2)	2·62
C(4)2/*A*	1·0590 (2)	0·4076 (1)	0·2520 (2)	1·58
H(4)2/*A*	1·090 (2)	0·442 (1)	0·324 (2)	1·98
C(5)2/*A*	1·0773 (2)	0·4257 (1)	0·1346 (2)	1·72
H(5)2/*A*	1·118 (2)	0·470 (1)	0·124 (2)	2·87
C(6)2/*A*	1·0327 (2)	0·3786 (1)	0·0371 (2)	1·75
H(6)2/*A*	1·042 (2)	0·388 (1)	−0·043 (2)	3·04
N(1)2/*B*	0·8487 (1)	0·1949 (1)	0·0622 (1)	1·39
C(2)2/*B*	0·8726 (1)	0·2335 (1)	0·1692 (2)	1·22
C(3)2/*B*	0·8202 (2)	0·2196 (1)	0·2683 (2)	1·58
H(3)2/*B*	0·839 (2)	0·248 (1)	0·342 (2)	3·12
C(4)2/*B*	0·7350 (2)	0·1645 (1)	0·2539 (2)	1·96
H(4)2/*B*	0·697 (2)	0·153 (1)	0·319 (2)	4·40
C(5)2/*B*	0·7075 (2)	0·1253 (1)	0·1433 (2)	1·85
H(5)2/*B*	0·647 (2)	0·090 (1)	0·126 (2)	2·84
C(6)2/*B*	0·7671 (2)	0·1419 (1)	0·0510 (2)	1·61
H(6)2/*B*	0·750 (2)	0·112 (1)	−0·028 (2)	1·78

based on user-defined blocks to the limit of the memory available. Crystal data and details of the refinement are given in Table 1.* Atomic coordinates and equivalent isotropic thermal parameters are listed in Table 2.

Structural geometry

The $B_{10}H_{10}$ moiety in both structures forms a bicapped square antiprism shown in Fig. 1. Neglecting distortion, the capping or apical B atoms in the cluster are chemically equivalent and distinct from the central B atoms of the antiprism. Allowing distortion of the bond lengths without loss of the cluster's symmetry, the apical and central B—H bonds differ, and three distinct B—B bonds exist.

The geometry of the YELLOW structure at 100 K closely resembles that determined by Fuller, Kepert, Skelton & White (1987) at 295 K. Distances from the apical to central atoms, from one capped square face of the antiprism to the other, and along the edges of each square face give the bond lengths grouped in Table 3(*a*). The cationic bond lengths of REDCOP are listed in Table 3(*b*), and those for YELLOW are listed in Table 3(*c*).

The REDCOP bipyridylium unit is *transoid* (Fig. 1*a*), with an interplanar dihedral angle of 44°. For YELLOW, the ring disposition is *cisoid* and almost planar, with interplanar dihedral angles of 0·2 (±1·4) and 16·8 (±0·2)° for the two independent cations compared with 1·3 and 16·4° for the room-temperature refinement.

* Lists of atomic coordinates, bond lengths and angles, and structure factors have been deposited with the British Library Document Supply Centre as Supplementary Publication No. SUP 51569 (49 pp.). Copies may be obtained through The Executive Secretary, International Union of Crystallography, 5 Abbey Square, Chester CH1 2HU, England.

Distances between the H atoms of the $B_{10}H_{10}$ cluster and those in the bipyridylium units are listed in Table 3(*d*). There are indications that the geometries of the interacting groups distort owing to the close contacts. In REDCOP the strong [1·91 (3) Å] contact H(4)···H(1)*A* appears to increase the B(4)–H(4) length to 1·14 (2) Å. The shorter [1·86 (3) Å] contact H(9)···H(1)*B* does not distort the cluster's geometry significantly. These two contacts are believed to be related to the intense charge-transfer spectra.

For YELLOW the close contacts are longer than those in REDCOP, as expected from its less intense charge-transfer spectrum. The two shortest contacts H(3)···H(1)2/*A* and H(6)···H(5)1/*B* are associated with the long N(1)–H(1)2/*A* and C(5)–H(5)1/*B* bonds respectively. Seven out of the nine contacts shorter than 2·41 Å involve the *A* end of the bipyridylium units, which contain the protonated N atoms. Those to the *B* end involve H(5) in both units. The B(1)–H(1), B(1)–B(5) and B(5)–H(5) bonds are significantly shorter than the others in the same class, presumably due to the effect of intermolecular interactions. The distances for each bipyridylium unit are not equivalent, so the charges transferred may differ.

Charge partitioning

Difference densities were evaluated for both data sets. The charges on each atom were calculated by partitioning the $\Delta\rho$ map into overlapping units with weights proportional to the free-atom, or promolecule, densities ρ at that point (Hirshfeld, 1977*a*,*b*). The sum extends beyond the asymmetric unit since contributions from atoms related by symmetry or cell translations may be significant for points near the edges of the map.

In a second partitioning the weights were based on free-atom electrostatic potentials v, calculated from the Hartree–Fock wavefunctions by Clementi & Roetti (1974). The potential has a long range compared to the density and a discontinuity at each atomic position resulting from the nuclear potential.

E.s.d.'s in the charges were estimated from the standard deviation of the integral of the difference density over a sphere, given by a simplified form of equation (8) of Davis & Maslen (1978):

$$\sigma^2(Q) = (4\pi R^3/V)^2 \times \sum\{[\sin(RS) - RS\cos(RS)]^2/(RS)^6\}\sigma^2(F),$$

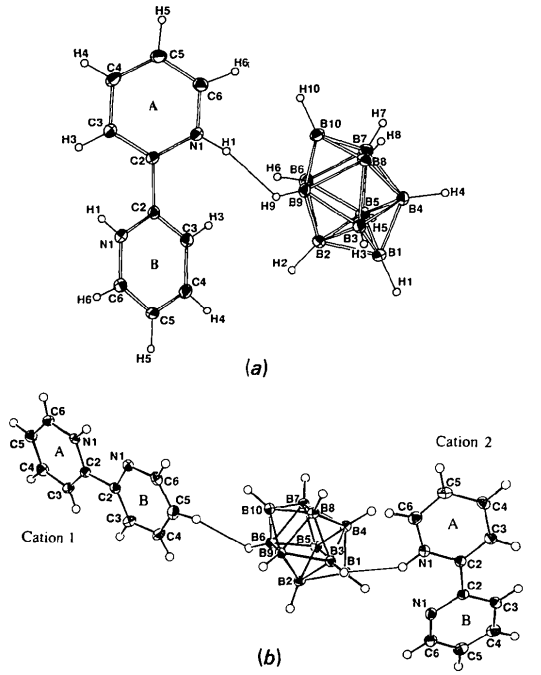

Fig. 1. The asymmetric unit for (*a*) REDCOP and (*b*) YELLOW.

Table 3. *Bond lengths* (Å)

(*a*) $B_{10}H_{10}$ clusters

	REDCOP	YELLOW		REDCOP	YELLOW
B(1)–B(2)	1·683 (4)	1·702 (3)	B(2)–B(3)	1·833 (4)	1·834 (3)
B(1)–B(3)	1·691 (4)	1·703 (3)	B(3)–B(4)	1·826 (4)	1·835 (3)
B(1)–B(4)	1·680 (3)	1·710 (3)	B(4)–B(5)	1·830 (4)	1·823 (3)
B(1)–B(5)	1·690 (5)	1·696 (3)	B(5)–B(2)	1·821 (4)	1·838 (3)
B(10)–B(6)	1·690 (4)	1·706 (3)	B(6)–B(7)	1·831 (4)	1·832 (3)
B(10)–B(7)	1·685 (4)	1·701 (3)	B(7)–B(8)	1·832 (4)	1·829 (3)
B(10)–B(8)	1·689 (4)	1·704 (3)	B(8)–B(9)	1·822 (4)	1·823 (3)
B(10)–B(9)	1·687 (4)	1·709 (3)	B(9)–B(6)	1·832 (4)	1·836 (3)
B(2)–B(6)	1·807 (4)	1·808 (3)	B(1)–H(1)	1·11 (2)	1·01 (2)
B(2)–B(9)	1·822 (3)	1·810 (3)	B(10)–H(10)	1·11 (2)	1·06 (2)
B(3)–B(8)	1·807 (4)	1·815 (3)			
B(3)–B(9)	1·798 (4)	1·815 (3)	B(2)–H(2)	1·10 (2)	1·08 (2)
B(4)–B(7)	1·824 (4)	1·810 (3)	B(3)–H(3)	1·12 (2)	1·09 (2)
B(4)–B(8)	1·807 (4)	1·806 (3)	B(4)–H(4)	1·14 (2)	1·07 (2)
B(5)–B(6)	1·831 (4)	1·816 (3)	B(5)–H(5)	1·10 (2)	1·00 (2)
B(5)–B(7)	1·811 (3)	1·811 (3)	B(6)–H(6)	1·11 (2)	1·10 (2)
			B(7)–H(7)	1·06 (2)	1·12 (2)
			B(8)–H(8)	1·07 (2)	1·09 (2)
			B(9)–H(9)	1·08 (2)	1·07 (2)

(*b*) REDCOP cation

	A	*B*		*A*	*B*
N(1)–H(1)	0·88 (2)	0·92 (3)	N(1)–C(2)	1·352 (3)	1·354 (3)
C(3)–H(3)	0·92 (2)	0·96 (2)	C(2)–C(3)	1·374 (3)	1·369 (3)
C(4)–H(4)	0·99 (2)	0·94 (2)	C(3)–C(4)	1·395 (3)	1·391 (3)
C(5)–H(5)	0·98 (2)	1·00 (2)	C(4)–C(5)	1·367 (4)	1·372 (3)
C(6)–H(6)	1·02 (2)	0·99 (2)	C(5)–C(6)	1·372 (3)	1·374 (4)
N(1)–C(6)	1·344 (3)	1·342 (3)	C(2)–C(2′)	1·480 (3)	

(*c*) YELLOW cation

	1/*A*	1/*B*	2/*A*	2/*B*
N(1)–H(1)	0·87 (2)		0·98 (2)	
C(3)–H(3)	0·91 (2)	0·95 (2)	0·94 (2)	0·95 (2)
C(4)–H(4)	0·99 (2)	0·95 (2)	1·01 (2)	0·95 (3)
C(5)–H(5)	0·94 (2)	1·01 (2)	0·95 (2)	0·94 (2)
C(6)–H(6)	0·96 (2)	0·91 (2)	0·93 (2)	1·00 (2)
N(1)–C(2)	1·348 (2)	1·350 (2)	1·342 (2)	1·345 (2)
N(1)–C(6)	1·336 (2)	1·334 (2)	1·346 (3)	1·337 (2)
C(2)–C(3)	1·385 (2)	1·387 (3)	1·383 (2)	1·388 (3)
C(3)–C(4)	1·384 (3)	1·394 (3)	1·391 (3)	1·392 (3)
C(4)–C(5)	1·392 (3)	1·386 (3)	1·395 (3)	1·386 (3)
C(5)–C(6)	1·382 (2)	1·391 (3)	1·381 (3)	1·386 (3)
C(2)–C(2′)	1·481 (2)		1·486 (2)	

(*d*) H–H intermolecular distances less than 2·4 Å

	REDCOP		YELLOW
H(9)···H(1)*B*	1·86 (3)	H(3)···H(1)2/*A*	2·14 (4)
H(4)···H(1)*A*	1·91 (3)	H(6)···H(5)1/*B*	2·25 (3)
H(1)···H(6)*A*	2·16 (3)	H(2)···H(1)1/*A*	2·30 (3)
H(10)···H(6)*B*	2·28 (3)	H(5)···H(5)1/*A*	2·31 (3)
H(8)···H(6)*B*	2·38 (3)	H(9)···H(3)2/*A*	2·36 (3)
		H(1)···H(6)1/*A*	2·36 (3)
		H(4)···H(5)2/*A*	2·37 (3)
		H(7)···H(4)1/*A*	2·37 (3)
		H(8)···H(5)2/*B*	2·40 (3)

Table 4. *Charges* (e) *on the boron cluster and bipyridylium cations*

Standard deviations are 0·02 and 0·07 e for atom and group charges respectively.

(*a*) Boron cluster

	REDCOP		YELLOW	
	ρ	v	ρ	v
B(1)	−0·08	−0·10	−0·09	−0·11
H(1)	−0·02	−0·01	−0·12	−0·07
B(2)	−0·01	−0·06	−0·07	−0·09
H(2)	−0·08	−0·04	−0·12	−0·06
B(3)	−0·13	−0·15	−0·04	−0·06
H(3)	−0·14	−0·07	−0·05	−0·04
B(4)	−0·07	−0·09	−0·09	−0·11
H(4)	−0·11	−0·05	−0·09	−0·04
B(5)	−0·19	−0·20	−0·04	−0·08
H(5)	−0·18	−0·10	−0·13	−0·08
B(6)	−0·16	−0·18	−0·04	−0·07
H(6)	−0·16	−0·09	−0·09	−0·04
B(7)	−0·01	−0·05	−0·05	−0·07
H(7)	−0·01	−0·01	−0·07	−0·04
B(8)	−0·12	−0·13	−0·06	−0·09
H(8)	−0·11	−0·06	−0·10	−0·05
B(9)	−0·10	−0·11	−0·03	−0·06
H(9)	−0·13	−0·06	−0·08	−0·04
B(10)	−0·02	−0·05	−0·11	−0·13
H(10)	−0·03	−0·02	−0·15	−0·08
Totals	−1·87	−1·62	−1·64	−1·41

(*b*) Bipyridylium cations

	REDCOP				YELLOW							
	A		*B*		1/*A*		1/*B*		2/*A*		2/*B*	
	ρ	v	ρ	v	ρ	v	ρ	v	ρ	v	ρ	v
N(1)	0·20	0·18	0·19	0·17	0·19	0·17	−0·09	−0·06	0·08	0·07	0·06	0·05
H(1)	0·11	0·06	0·12	0·06	0·02	0·02			0·05	0·03		
C(2)	0·11	0·11	0·12	0·11	0·08	0·08	0·03	0·03	0·10	0·08	0·16	0·11
C(3)	0·10	0·08	0·01	0·00	0·04	0·04	0·07	0·06	−0·06	−0·06	−0·00	−0·00
H(3)	−0·04	−0·01	−0·05	−0·03	−0·03	−0·01	0·06	0·03	−0·08	−0·05	0·05	0·03
C(4)	0·15	0·14	0·05	0·04	0·02	0·02	0·01	0·01	0·00	0·00	0·08	0·06
H(4)	0·07	0·05	0·00	0·00	0·02	0·02	−0·05	−0·02	0·07	0·04	−0·03	−0·02
C(5)	0·15	0·16	0·10	0·09	0·11	0·09	0·07	0·08	−0·00	0·00	0·06	0·01
H(5)	0·11	0·06	0·05	0·03	−0·01	−0·01	0·09	0·04	0·02	0·01	−0·01	−0·01
C(6)	0·14	0·14	0·10	0·10	0·15	0·14	0·15	0·10	0·10	0·08	0·10	0·09
H(6)	0·05	0·04	0·04	0·03	0·06	0·04	−0·02	−0·01	−0·01	−0·00	0·03	0·03

Totals	REDCOP cation		YELLOW cation 1		YELLOW cation 2	
	ρ	v	ρ	v	ρ	v
	1·87	1·62	0·97	0·87	0·67	0·54

where V is the volume of the unit cell and S is the length of the reciprocal lattice vector ($4\pi\sin\theta/\lambda$). R, the mean radius for an atom or group in the unit, is calculated from the number of atoms and the unit-cell volume. The variance changes slowly with atom radius, and is insensitive to the definition used.

Although differences between the two methods are statistically significant, both methods reveal the same broad trends, and the charges listed in Table 4 have approximately the same magnitudes. The atomic charges have a maximum magnitude of 0·20 e. The H atoms are systematically nearer to neutral for partitioning based on potentials but the B atoms acquire larger negative charges. Contributions to heavier atoms are increased at the expense of those for the H atoms as a result of the longer range of the promolecular potential.

With potential partitioning the group charges are less by approximately 0·2 e. The contributions from boron and hydrogen to the charges of the $B_{10}H_{10}^{2-}$ moiety in REDCOP change from −0·90 and −0·97 e respectively, with density partitioning, to −1·12 and −0·52 e for the subdivision based on potential. The values for YELLOW show the same trends.

The total charges with density paritioning, such as −1·87 e for the $B_{10}H_{10}^{2-}$ moiety in REDCOP and −1·64 e for YELLOW are close to the formal charge of −2e. The results show that the $B_{10}H_{10}$ cluster forms a stable, robust ionic species, with static charge transfer between large molecular units in the structure.

The results indicate that the charges on the two moieties in YELLOW differ. Although unit 2 has the shorter NHHB contact it has the smaller charge (~+0·6 e). Unit 1, with contacts to the neighbouring H(1) and H(6) atoms similar to the arrangement in REDCOP, has a charge just slightly less than its formal value of +1. This suggests that the B(1)–H(1)···H(6)–C(6) interaction makes a significant contribution to the charge transfer. This vector to unit 1, which has a length of 2·36 Å, is the only short contact involving an apical B atom in YELLOW. The other apical site has no contact within 2·70 Å. This unit has the larger number of H–H contacts (four) to the *A* end

of the molecule. It also has the stronger interaction with the *B* end of the molecule, which is reflected in the larger positive charge on C(5)–H(5).

The C atoms in the bipyridylium units carry larger charges than the H atoms. Those on the protonated N atoms are more positive and close to 0·2 e for REDCOP and for the *A* ring in unit 1 of YELLOW. The largest positive charges in the bipyridylium moieties are carried by the N atoms close to the boron clusters but the non-protonated N in unit 1 of YELLOW is negatively charged. For the monoprotonated ring 2/*B* with weaker contacts the atomic charges are smaller. A large fraction of the charge is carried by the central C(2) atom in that unit.

Other methods for estimating atomic charges applied to boron clusters and similar species include the refinement of electron populations in density basis sets and radial integration of the total density out to a fixed radius or surface (Ito & Higashi, 1983; Bader & Messer, 1974). The former technique provides information relevant to postulated sets of orbitals but frequently overestimates atomic charges. Partitionings of the total electron density are subject to the difficulties described by Maslen & Spackman (1985).

Previous density distribution partitionings using Hirshfeld's method (*e.g.* Hirshfeld & Hope, 1980; Hirshfeld, 1984) gave physically reasonable estimates of charges in multiply bonded atoms and non-polar molecules. This study confirms that large charges can be transferred between species in crystals despite the individual atomic charges being relatively small.

Difference density

The more detailed difference density is that for the extensive low-temperature data set for YELLOW. The value of 0·08 e Å^{-3} for $\sigma(\Delta\rho)$ is an incomplete measure of the significance of a feature in the map. The geometry of the isolated $B_{10}H_{10}$ moiety has high symmetry, which is conserved quite closely in the crystal. This symmetry should be reflected in the deformation density (the redistribution of electron density due to bonding), except where it is perturbed by strong intermolecular contacts. The extent to which the difference density shows this symmetry is a guide to how accurately it represents the deformation density.

Sections of the difference density through each triangular face of the boron clusters were studied. Neglecting asymmetric features caused by close contacts, two classes of faces are expected. Apical triangular faces, involving a capping B atom and two adjacent central B atoms, should have a mirror symmetry about the axis through the capping atom to the midpoint of the edge of the antiprism. Central triangular faces from a central B atom to the two B atoms on the other square face of the antiprism should also show approximate mirror symmetry. Although there is considerable variation between the densities for the different types of B_3 rings, there is approximate mirror symmetry in almost all cases. It is therefore appropriate to average the maps across mirror planes containing the B(1)–B(10) axis, denoted 1*m* averaging, as in Figs. 2 and 3.

In the averaging, the centroid and the midpoint of the edge with the highest symmetry lies on the mirror plane. The method is essentially that of Ito, Higashi & Sakurai (1979), whose maps for the B_3 rings closely resemble those reported here.

The most important feature in Fig. 2 is a peak near the edges from the apical to the central B atoms. The positive density at the centre of the face is an extension

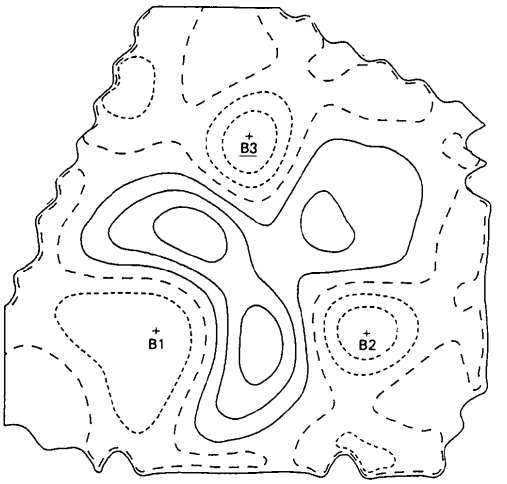

Fig. 2. Difference density maps of triangular faces of the boron cluster – 1*m*-average of all apical faces of the YELLOW cluster. Contours at 0·05 e Å^{-3} intervals. Negative contours broken. Map dimensions 3·9 × 3·75 Å.

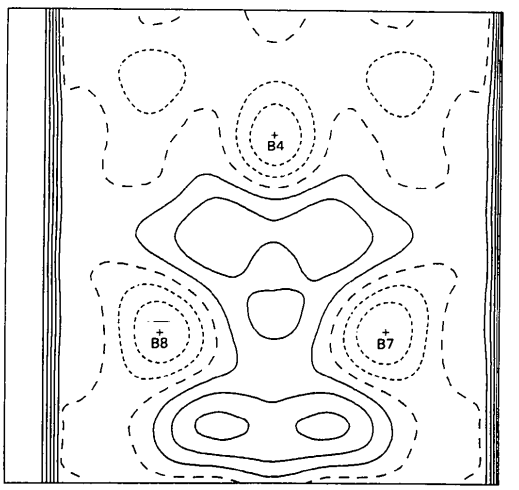

Fig. 3. 1*m*-Average of central faces of YELLOW. Contours as in Fig. 2. Map dimensions 3·9 × 3·75 Å.

of the peaks along the edges. Density has migrated from near the atom sites to the cluster as a whole. The map for the central faces of REDCOP, shown in Fig. 4, has a central peak in addition to peaks along and outside the triangular edges which are of approximately equal size. The bulk of the electron density has migrated outside the edge of the antiprism. There are similar features in the map for the apical faces.

Averaged axial planes through both apical B atoms and two central atoms for the YELLOW and REDCOP clusters are shown in Figs. 5 and 6. In Fig. 6, for REDCOP, there is a local dipole at each apical atom, along with B–H bonding peaks for the atoms. On the other hand the density near all B–H bonds for YELLOW in the averaged map (Fig. 5), is featureless. We are grateful to a referee for pointing out that this may be consistent with the effects of thermal anharmonicity being larger in the room-temperature REDCOP structure.

There are large hollows at the centre of the cluster in both maps. For YELLOW this is a double hollow which is important with regard to bonding theories for boron clusters. In REDCOP the deepest minimum lies closer to the B(10) apical atom. If open-centre B_3 bonding contributed toward the cohesion of the structure, there should be peaks inside the cluster and near the central atom of this open bond. However, no such peak was observed in any axial map for either structure.

For the axial planes for YELLOW, the location of the major peaks of electron density at the triangular faces of the cluster is particularly prominent. In REDCOP these features are smaller but still appreciable. There are three other connected peaks in the YELLOW map, corresponding to positions (*a*) outside the central faces; (*b*) outside the midpoints of the edges of the square faces of the antiprism; and (*c*) above the apical faces. For REDCOP (*c*) is especially prominent while (*a*) is missing. In so far as bonding in B–H species is characterized by the accumulation of electron density, the maps indicate that there are bonds along apical edges and above apical faces, with weaker features above central faces and edges.

The results may be compared with the difference density distribution in related systems such as *cis*-1,2,3-tricyanocyclopropane (Hartman & Hirshfeld, 1966), for which the strained ring has large peaks outside the edges, and a central hollow. The faces of the boron cluster described above also show concentration of density outside the triangle. This disposition is often described as resulting from the strain in the ring system.

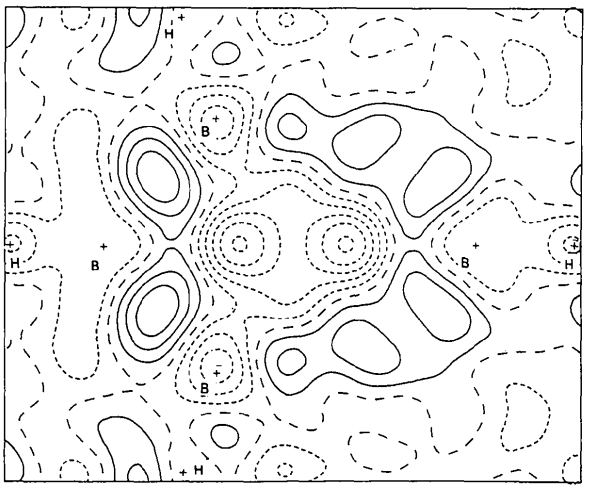

Fig. 5. 1*m*-Average of maps for the boron cluster of YELLOW. The apical B atoms are located on the symmetry axis in the individual maps and a B–B edge is included in each map. Contours as in Fig. 2. Map dimensions 5·85 × 4·80 Å.

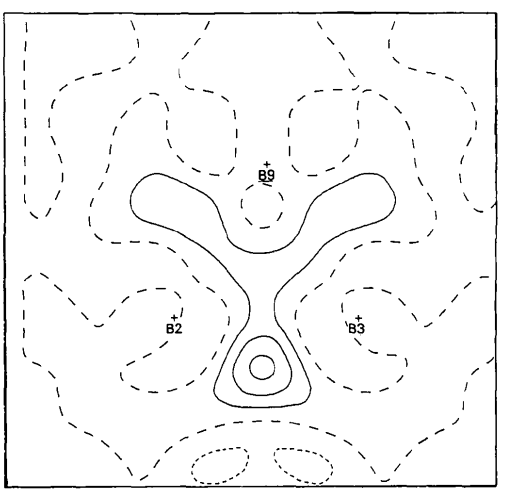

Fig. 4. 1*m*-Average of central faces for REDCOP. Contours as in Fig. 2. Map dimensions 5·027 × 4·834 Å.

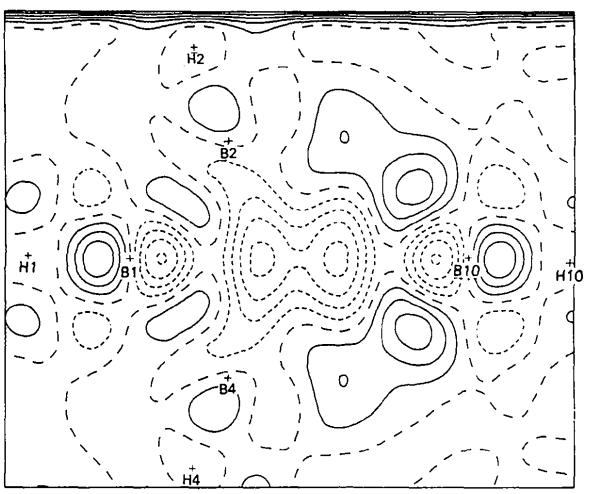

Fig. 6. 1*m*-Average maps for the boron cluster and apical B-atom positions of REDCOP. Contours as in Fig. 2. Map dimensions 6·187 × 5·221 Å.

Attributing such relocation of density to strain in the triangular face rather than to a three-centre bond appears arbitrary, especially as there is a peak on some faces. However, it is just as questionable to attribute the features observed to particular orbitals claimed to characterize the bonding.

The density in the strained ring system may be related to that in the boron cluster as a whole, by comparing the difference density in the ring to that of the axial planes through the cluster. There are hollows both in the strained ring and inside the cluster, with peaks on and outside the faces and edges of the cluster and the ring (Figs. 5 and 6). Electron density is transferred from the electron-rich regions where several atoms overlap to less-electron-rich regions outside the molecule. Such movement away from electron-rich regions is typical of fermions and an expected consequence of antisymmetrizing the atomic wavefunctions when forming the structure, *i.e.* of exchange.

For the bipyridylium group the deformation density in the rings (not shown) has peaks on the bonds for both structures, which are more prominent for the low-temperature structure with the more extensive data, as expected. Peaks corresponding to the C—C bond between the rings and to lone pairs outside the N atoms in the monoprotonated species are clear, as expected. The hollows are deep and the peaks are small, as is expected since the bipyridylium units are positively charged.

There are asymmetric features corresponding to asymmetric close intermolecular contacts as illustrated in Fig. 7. The peak at the bottom left-hand corner, lying roughly between the B(1)—B(4) apical edge and the N(1)*B* atom of the closest bipyridylium unit in REDCOP, is as large as any other feature in the map. It is not collinear with the H(4)···H(1)*B* close contact, suggesting that the charge transfer arises from an interaction localizable to the B and N atoms for the ring and cluster as a whole, and is not specific to the hydrogen contact alone. The close approach of the hydrogen could well result from the N—B interaction. The corresponding YELLOW maps have peaks with more complex shapes in this region, as expected because of the greater number of close contacts in the monoprotonated structure.

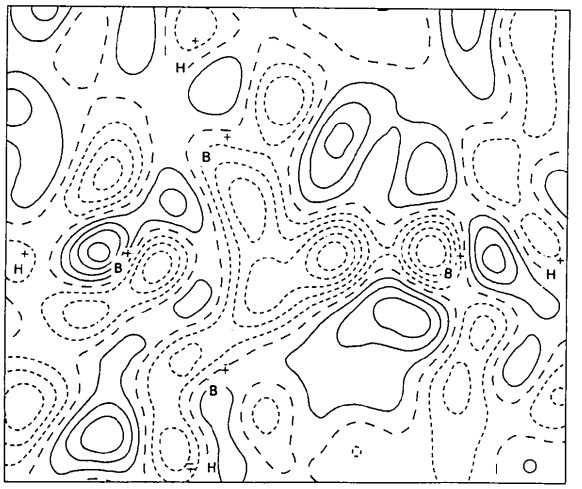

Fig. 7. Axial map through the centre of the REDCOP boron cluster, the apical B-atom positions and B(2) showing the asymmetric peak below B(1). Contours as in Fig. 2. Map dimensions 6·187 × 5·221 Å.

The authors acknowledge Professor Allan White and Dr Brian Skelton for their role in the data collection, and Professor Syd Hall for assistance with the programs used in this study. This work was supported by the Australian Research Grants Scheme.

References

BADER, R. F. W. & MESSER, R. R. (1974). *Can. J. Chem.* **52**, 2268–2282.

CLEMENTI, E. & ROETTI, C. (1974). *At. Data Nucl. Data Tables*, **14**, 177–478.

DAVIS, C. L. & MASLEN, E. N. (1978). *Acta Cryst.* A**34**, 743–746.

DIXON, D. A., KLIER, D. A., HALGREN, T. A., HALL, J. H. & LIPSCOMB, W. N. (1977). *J. Am. Chem. Soc.* **99**, 6226–6237.

FULLER, D. J. & KEPERT, D. L. (1983). *Polyhedron*, **2**, 749–759.

FULLER, D. J., KEPERT, D. L., SKELTON, B. W. & WHITE, A. H. (1987). *Aust. J. Chem.* **40**, 2097–2105.

HARTMAN, A. & HIRSHFELD, F. L. (1966). *Acta Cryst.* **20**, 80–82.

HIRSHFELD, F. L. (1977*a*). *Isr. J. Chem.* **16**, 198–201.

HIRSHFELD, F. L. (1977*b*). *Theor. Chim. Acta*, **44**, 129–138.

HIRSHFELD, F. L. (1984). *Acta Cryst.* B**40**, 484–492.

HIRSHFELD, F. L. & HOPE, H. (1980). *Acta Cryst.* B**36**, 406–415.

ITO, T. & HIGASHI, I. (1983). *Acta Cryst.* B**39**, 239–243.

ITO, T., HIGASHI, I. & SAKURAI, T. (1979). *J. Solid State Chem.* **28**, 171–184.

LARSON, A. C. (1970). *Crystallographic Computing*, edited by F. R. AHMED, pp. 209–213. Copenhagen: Munksgaard.

LONGUET-HIGGINS, H. C. (1949). *J. Chim. Phys. Phys.-Chim. Biol.* **46**, 268.

MASLEN, E. N. & RIDOUT, S. C. (1987). *Acta Cryst.* B**43**, 352–356.

MASLEN, E. N., RIDOUT, S. C. & WATSON, K. J. (1988). *Acta Cryst.* B**44**, 102–107.

MASLEN, E. N. & SPACKMAN, M. A. (1985). *Aust. J. Phys.* **38**, 273–287.

MUETTERTIES, E. L., BALTHIS, J. H., CHIA, Y. T., KNOTH, W. H. & MILLER, H. C. (1964). *Inorg. Chem.* **3**, 444–451.

SPADACCINI, N. (1988). PhD Thesis, Univ. of Western Australia, Australia.

STEWART, J. M. & HALL, S. R. (1986). *The XTAL System of Crystallographic Programs: User's Manual*, version of December 1983. Tech. Rep. TR-1364. Computer Science Center, Univ. of Maryland, College Park, Maryland, USA.

STONE, A. J. (1981). *Inorg. Chem.* **20**, 563–571.

ZACHARIASEN, W. (1967). *Acta Cryst.* **18**, 558–564.